MICHIGAN STATE UNIVERSITY

CYCLOTRON LABORATORY

SURFACE RESPONSE OF FERMI LIQUIDS

H. ESBENSEN and G. F. BERTSCH

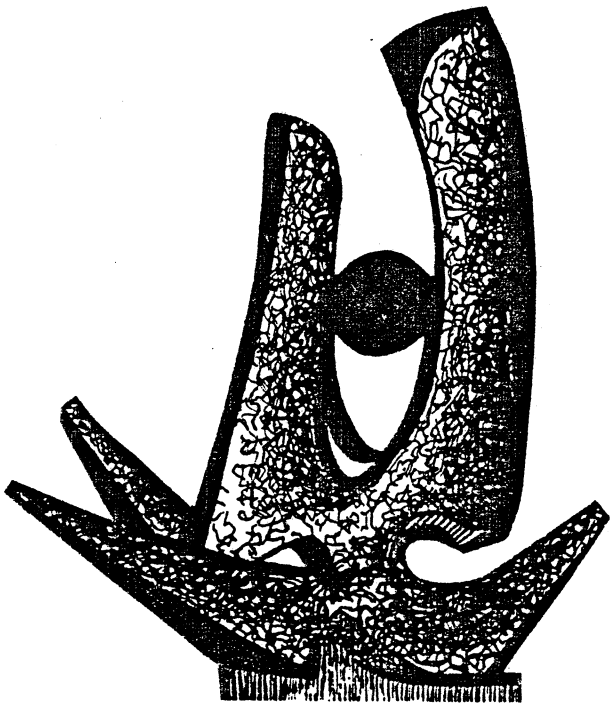

JANUARY 1984

MSUCL-445

MSUCL-445
January 1984

Surface Response of Fermi Liquids.

H. Esbensen and G. F. Bertsch

Cyclotron Laboratory and Physics Department

Michigan State University

East Lansing, MI 48824

Abstract. We calculate the response of a semi-infinite self-bound Fermi liquid to a surface field using the random phase approximation, with specific application to the nuclear surface. A separable approximation for the induced field is found to be quite accurate. There is a divergence in the isoscalar response at zero frequency associated with the translational degeneracy of the system, but quantities such as the energy-weighted strength, the surface tension and the zero-point fluctuation of the surface density are well behaved. The theory is applied to the inelastic scattering of protons from nuclei, and we find that the nuclear response is well reproduced by the semi-infinite theory.

Contents:

1. Introduction.

The Random Phase Approximation (RPA) is a remarkably accurate theory of the response of systems of interacting fermions. For translationally invariant systems, the long wavelength limit provides the Landau theory of Fermi liquids, a useful theory for the bulk properties of nuclear matter, liquid ^{3}He, and electrons in simple metals. In a spherical representation, the RPA provides a description of nuclear excitation properties, which is useful even for detailed spectroscopy of excited states.

In this work we consider another limit of RPA, the theory of the surface response of semi-infinite systems. Many physical probes emphasize the surface response of the medium. For example, the scattering of hadrons from nuclei probes a region of the nuclear surface whose depth is of the order of the surface thickness. In low energy electron scattering from metals, the surface modes play an important role.

The RPA theory of semi-infinite Fermi systems has been developed for electrons in metals [1-3], and also investigated for the nuclear surface [4]. However, there are numerous questions about the surface response that have not been properly addressed, particularly for self-bound Fermi systems such as nuclei. Some questions we will try to answer include:

(1) are there new features in the surface response qualitatively different from the bulk response?

(2) how accurate are simplified models, such as the Thomas-Fermi model, for characterizing the surface response?

(3) is the empirically measured response adequately described by the RPA theory?

Before we can address these questions, we need to establish an RPA formalism, which is done in the next Section. By making simplifying

assumptions about the interactions, we can construct a solvable model for the surface response. The simplified model is compared with numerical solutions of the integral equation in Section 3.

We shall find that self-bound Fermi systems do indeed exhibit surface response features different from the bulk behavior. In other aspects, the surface response is close to the bulk response at an appropriate density. The comparison to the Thomas-Fermi and other simple treatments is made in Section 4. In section 5 an effective surface tension is extracted from the static surface polarization. Finally, in Section 6 we compare the RPA with some empirical energy-loss scattering measurements, finding good agreement.

2. The Slab Model.

We begin with a model of the ground state of a semi-infinite slab. The wavefunction is a product of independent particle wavefunctions, chosen as eigenstates of a single-particle Hamiltonian. The medium occupies the z<0 half-space with the surface in the x-y plane. The single particle wavefunctions will be plane waves in the x-y directions, and have a z-dependence which must be calculated numerically from the Hamiltonian

$$H_0 = -\frac{\hbar^2}{2m}\vec{\nabla}^2 + V(z). \tag{2.1}$$

We shall not go through the Hartree-Fock procedure to determine the single particle potential V(z) from the interaction via the self-consistent equations. Rather, we will choose V(z) in a phenomenological way as a Fermi function

$$V(z) = V_0\,(1 + \exp(-z/a))^{-1}, \tag{2.2}$$

and use the self-consistency of the Hartree-Fock to constrain the interaction in the RPA equation.

2.1 The RPA Equation.

For purposes of establishing notation, we shall remind the reader of the RPA theory. The collective response is conveniently formulated as an integral equation for the induced density $\delta\rho$. The source term is an external perturbation $U(\vec{r})\cos(\omega t)$ that is periodic in time. Through the residual interaction $\mathcal{V}$ the induced density generates the induced potential

$$\delta V(\vec{r},\omega) = \int d\vec{r}'\, \mathcal{V}(\vec{r},\vec{r}')\, \delta\rho(\vec{r}',\omega). \tag{2.3}$$

The self-consistent induced density is thus determined by

$$\delta\rho(\vec{r},\omega) = -\int d\vec{r}'\, G_0(\vec{r},\vec{r}',\omega)\,\{\, U(\vec{r}') + \delta V(\vec{r}',\omega)\,\}, \tag{2.4}$$

where G_0 is the field-free Green's function, obtained from first order perturbation theory. The construction of G_0 and the single-particle density

$\rho_0(z)$ in the non-interacting ground state for slab geometry is described in Appendix A. The formal solution is expressed by the RPA Green's function

$$\delta\rho = -G_{RPA}\,U = -(1+G_0\mathcal{V})^{-1}\,G_0\,U. \tag{2.5}$$

Various approximations for the residual interactions are discussed in section 2.4. We shall always assume that they are translationally invariant in the coordinates measured along the surface of the slab. All Green's functions are then also translationally invariant in these directions, and it is convenient to introduce their Fourier representation

$$G(\vec{r},\vec{r}',\omega) = (2\pi)^{-2}\int d^2\vec{K}\; G(z,z',K,\omega)\,\exp(i\vec{K}(\vec{r}_p-\vec{r}_p')). \tag{2.6}$$

Here $\vec{r}_p$ and $\vec{r}_p'$ are coordinate vectors parallel to the surface, and $\vec{K}$ is the associated Fourier vector. The Green's functions $G(z,z',K,\omega)$ are independent of the orientation of $\vec{K}$, (c.f. Appendix A).

2.2 Response Functions.

We next must specify the form of the external field U. This will depend on the characteristics of the external probe, in particular how strongly the probe is absorbed by scattering processes. For discussing the general features of the response it is useful to define a particular external field, proportional to the derivative of the single-particle potential

$$U(\vec{r}) = -V'(z)\,\exp(i\vec{K}\vec{r}_p). \tag{2.7}$$

The response of the system is then a function of two parameters, viz. the momentum transfer $\hbar K$ along the surface and the excitation energy $\hbar\omega$. Note that K plays a similar role as the multipolarity does for spherical nuclei. The response function is defined as

$$S(K,\omega) = \frac{1}{\pi}\,\mathrm{Im}\{\int dz \int dz'\; V'(z)\; G(z,z',K,\omega)\; V'(z')\}. \tag{2.8}$$

The response function is determined by excitations of the system that are on the energy-shell. The off-energy-shell transitions are contained in

the real part of the Green's function, and they are associated with polarizations of the system. To make this destinction between the response and polarizations quite clear we define the dynamic polarization function as follows

$$P(K,\omega) = \mathrm{Re}\{\int dz \int dz'\ V'(z)\ G(z,z',K,\omega)\ V'(z')\}. \qquad (2.9)$$

Various sum rules for the response are given in section 2.5.

2.3 RPA for Separable Interactions.

For a general residual interaction $\mathcal{V}$ the inversion of the matrix $1+G_0\mathcal{V}$ in Eq. (2.5) is complicated by the fact that perturbations induced by the external field will propagate into the interior of the slab, and bulk oscillations of the induced density can again affect the collective surface response through a strong residual interaction. Using a separable residual interaction, however, one can easily obtain the RPA response from the free response. For simplicity we choose the separable interaction

$$\mathcal{V}(\vec{r},\vec{r}') = \kappa_0\ V'(z)\ V'(z')\ g(\vec{r}_p-\vec{r}'_p), \qquad (2.10)$$

where the function g describes the interaction in directions parallel to the surface, and the coupling strength κ_0 can be adjusted in order to simulate more realistic interactions as discussed in the next section. In the Fourier representation for slab geometry this interaction becomes

$$\mathcal{V}(z,z',K) = \kappa(K)\ V'(z)\ V'(z'), \qquad (2.11)$$

where the K-dependent coupling strength is $\kappa(K)=\kappa_0 g(K)$, and we normalize $g(K=0) = 1$. The RPA Green's function can then be obtained from the expansion

$$\begin{aligned} G_{RPA} &= G_0 - G_0\mathcal{V}G_0 + G_0\mathcal{V}G_0\mathcal{V}G_0 - \ldots \\ &= G_0 - \kappa\ (G_0V')(V'G_0)\ \{1+\kappa(V'G_0V')\}^{-1}. \end{aligned} \qquad (2.12)$$

The induced density of the collective response can be obtained from the field-free induced density $\delta\rho_0$ by

$$\delta\rho_{RPA}(z,K,\omega) = \delta\rho_0(z,K,\omega)\ \{1+\kappa(V'G_0(K,\omega)V')\}^{-1}. \qquad (2.13)$$

The RPA response can be expressed in terms of the field-free response S_0 and the field-free polarization function P_0 as follows

$$S_{RPA}(K,\omega) = S_0(K,\omega)\ \{(1+\kappa P_0(K,\omega))^2 + (\kappa\pi S_0(K,\omega))^2\}^{-1}. \qquad (2.14)$$

The RPA response for separable interactions is completely determined by the coupling constant κ and the free response, since the polarization function can be obtained from the response function through the Kramers-Kronig relation (2.26).

2.4 Residual Interactions.

We determine the isoscalar coupling strength κ_0 from the requirement that an induced density of the form $\delta\rho(z) = -\rho_0'(z)\delta z$ leads to a similar induced potential $\delta V(z) = -V'(z)\delta z$ through the residual interaction. This condition would follow automatically from a self-consistent Hartree-Fock calculation. The self-consistency requirement applied to Eqs. (2.3) and (2.11) yields

$$\kappa_0^{-1} = \int dz\ \rho_0'(z)\ V'(z) = -\int dz\ \rho_0(z)\ V''(z), \qquad (2.15)$$

which implies that the isoscalar response diverges in the static limit for K=0. To demonstrate this point we note that a static displacement of the single particle potential leads to the same displacement of the slab density. In first order perturbation theory one finds in particular (c.f. Appendix C, Eq. (C.6))

$$\delta\rho_0(z,K=0,\omega=0) = \int dz'\ G_0(z,z',0,0)\ V'(z') = -\rho_0'(z). \qquad (2.16)$$

The associated value of the field-free polarization function is

$$P_0(K=0,\omega=0) = -\int dz\ V'(z)\ \rho_0'(z) = \int dz\ \rho_0(z)\ V''(z) \qquad (2.17)$$

The first term in the denominator of (2.14) then vanishes in the static limit. Moreover, the free response vanishes linearly in ω in this limit as we shall see, and it follows that the RPA response will diverge as $1/\omega$ for $\omega \to 0$. A similar result is found for spherical nuclei, where the spurious isoscalar dipole mode is located at zero excitation energy. For non-zero values of K the isoscalar response is more well behaved with a vanishing response at $\omega=0$.

More realistic interactions, as for example the Skyrme type commonly used in Hartree-Fock calculations, has zero range and contain a density dependence. We shall therefore also study the response using interactions of the form

$$\mathcal{V}(\vec{r},\vec{r}') = v_c(z)\,\delta^{(3)}(\vec{r}-\vec{r}'). \qquad (2.18)$$

The position dependence is ascribed to a density dependence in the effective interaction that could be calculated in Brueckner Hartree-Fock theory. Because of the zero range in (2.18), the function $v_c(z)$ in the isoscalar channel is determined by the self-consistency condition to be

$$v_c(z) = V'(z)/\rho_0'(z).$$

In the surface region a good fit is given by the function

$$v_c(z) = -50 - 500/(1+\exp(-z(\mathrm{fm})/0.5)) \quad \mathrm{MeV\ fm}^3. \qquad (2.19)$$

Notice that the interaction is very attractive in the far surface, and that it practically vanishes in the interior.

For most of our calculations we assume that the interaction has zero range in directions parallel to the surface. The coupling constant $\kappa(K)$ for the separable interaction (2.11) is then independent of K. For the isoscalar mode we shall also study the effect of a finite range. Using a Yukawa interaction of range a_r, the K-dependence of the coupling constant is

$$\kappa(K) = \kappa_0\,\left|1+(Ka_r)^2\right|^{-1/2}, \qquad (2.20)$$

where κ_0 is determined by Eq. (2.15).

No self-consistency argument can be used to determine the interactions for the isovector and the spin modes. We adopt again the parametrization (2.18) for each of these interactions, but ignore a position dependence of v_c, which seems reasonable from empirical studies of the response of finite nuclei. The coupling strength of the corresponding separable interaction is set by demanding that it has the same diagonal matrix elements as the microscopic interaction. This leads to the value

$$\kappa = v_c\,\left\{\int dz\ (V'(z))^2\right\}^{-1}. \qquad (2.21)$$

Numerical studies of the Gamow-Teller response [5] show that existing experimental data are well reproduced using the interaction (2.18) with v_c= 220 MeV fm^3 for the (T=1,S=1) channel. Similar studies of the isobaric analog state and the giant dipole resonance [6] indicate that the isovector channel can be described by the interaction (2.18) with v_c= 300 MeV fm^3. The residual interaction in the (T=0,S=1) channel is much weaker than in the (T=1,S=0) channel. We adopt the numerical value v_c= 50 MeV fm^3 in section 6.

2.5 Sum Rules.

It is useful to define a new response function, the direct response, for our discussion of the sum rules. Similar to Eq. (2.8) we define the direct response

$$S_0^D(K,\omega) = \frac{1}{\pi}\,\mathrm{Im}\left\{\int dz \int dz'\ V'(z)\,G_0^D(z,z',K,\omega)\,V'(z')\right\}, \qquad (2.22)$$

where the direct field-free Green's function G_0^D is defined in appendix A, Eq. (A.9). This response does not respect the Pauli principle, and it is non-zero for all transitions down to minus the Fermi energy. The free response, obtained from the retarded field-free Green's function (A.6), can be constructed from the direct response as follows

$$S_0(K,\omega) = S_0^D(K,\omega) - S_0^D(K,-\omega). \tag{2.23}$$

The second term cancels all forbidden transitions contained in the direct response, so that the Pauli principle is obeyed. This response is an odd function of ω, and all poles in the complex ω-plane are below the real axis, characteristic for a retarded response. For the particular type of residual interactions considered in the previous section that all commute with the external field (2.7), one finds [7] that the energy-weighted sum rule (EWSR) for the RPA response is identical to the EWSR of the free response, and it is given by

$$\hbar^2 \int_0^\infty d\omega\, \omega S(K,\omega) = \frac{\hbar^2}{2m} \int dz\, \rho_0(z) \left[(V''(z))^2 + K^2 (V'(z))^2 \right]. \tag{2.24}$$

The direct response function has the normalization

$$\hbar \int_{-\infty}^\infty d\omega\, S_0^D(K,\omega) = \int dz\, \rho_0(z)\, (V'(z))^2. \tag{2.25}$$

There is no analogous simple sum rule for the total RPA or for the total free response, integrated over all positive excitation energies. The total free response is reduced compared to (2.25) due to the Pauli blocking, and the total RPA response depends strongly on the type of residual interaction being used.

Another important sum rule gives the connection between the response function and the dynamic polarization function (2.9). This is the Kramers-Kronig relation, which states that

$$P(K,\omega) = \int_{-\infty}^\infty d\omega'\, S(K,\omega') \frac{1}{2} \left[\frac{1}{\omega' - i\eta - \omega} + \frac{1}{\omega' + i\eta - \omega} \right]. \tag{2.26}$$

The second factor in the integrand is the principal value of $1/(\omega'-\omega)$. All the poles of a retarded response are below the real axis in the complex ω-plane, so we can close the ω'-integration by a semi-circle in the upper complex plane. The only pole inside this integration path is $\omega' = \omega + i\eta$, and

the result (2.26) follows directly. We shall later use this relation to obtain analytic approximations for the collective response. In particular, for K=0 we obtain the closed expression

$$\int_{-\infty}^\infty d\omega\, \frac{1}{\omega} S_0(K=0,\omega) = \int dz\, \rho_0(z)\, V''(z) \tag{2.27}$$

from the static polarization (2.17) of the non-interacting ground state.

3. Results of numerical Calculations.

In this section we study the response of a semi-infinite slab as a function of the excitation energy $\hbar\omega$ and the momentum transfer $\hbar K$ along the surface. The external field U is given in Eq. (2.7). To give this field the dimension of energy we shall always multiply it by 1 fm in displaying our results. We use the parameters $V_0 = 45$ MeV and $a = 0.75$ fm for the single-particle potential (2.2) in order to simulate the surface properties of heavy nuclei. The field-free Green's function given in Appendix A is calculated on a grid with a step size of 0.25 to 0.5 fm. The integration over the Fermi sphere is performed with a step size of 0.01 to 0.05 fm^{-1} in the z-direction perpendicular to the surface and in the x-direction parallel to the momentum transfer $\hbar\vec{K}$, whereas the integration over the remaining surface direction is trivial.

3.1 Results for K=0.

We consider first the collective response (2.14) for separable residual interactions in the limit K=0. The coupling strengths for the isoscalar and isovector interactions are given in Eqs. (2.15) and (2.21), respectively, and the results are shown in Fig. 1 together with the free response.

The isoscalar response is seen to be enhanced for $\hbar\omega < 10$ MeV compared to the free response. In this region it exhausts about 25% of the energy-weighted sum rule (EWSR), whereas the free response only contains 7.5% of the EWSR in this interval. Moreover, it diverges as $1/\omega$ for $\omega \to 0$, since we have adjusted the coupling strength from self-consistency.

The isovector response, on the other hand, is enhanced for large and reduced for small excitation energies compared to the free response. Thus the maximum occurs at an 8 MeV higher excitation energy than in the free

response. For all three response functions shown in Fig. 1 the EWSR is the same and it is given by Eq. (2.24).

The numerical calculation of the collective response, using the zero-range residual interactions (2.18) is more difficult, since the calculation of the RPA Green's function (2.5) involves a non-trivial inversion of the operator $1+G_0\mathcal{V}$. The inversion can be performed conveniently in coordinate space for spherical nuclei [7]. For slab geometry one finds that the induced density of the free response is so large in the interior of the slab that the associated induced potential becomes significant deep inside the slab surface. One would therefore need a very large interval in coordinate space to obtain reliable numerical results. To overcome this problem we used a finite damping of $\Delta = 2$ MeV in the field-free Green's function, and it was then sufficient to perform the numerical calculation on a finite interval that reaches 20-40 fm inside the slab surface. The results for the isoscalar and isovector responses are shown in Fig. 2, together with the response functions for separable interactions, all obtained with the damping width mentioned above. The two types of interactions are seen to yield quite similar responses.

To illustrate in more detail the effect of the zero-range residual interactions (2.18) we show in Fig. 3 the associated induced densities at an excitation energy of 15 MeV. For the isovector mode we see that the period of the interior oscillations is much larger and that the surface peak is much more smeared out than in the case of the free response, whereas the oscillations in the isoscalar density have shorter wave lengths and are enhanced near the surface. This is just the behavior one expects for the response of an infinite gas. The induced densities for the separable interactions, which are not shown, deviate from the density of the free

response mainly in the magnitude of the amplitudes. The periods of the interior oscillations are about the same as for the free response.

3.2 Lorentzian Approximation.

The free response discussed in the previous section is quite accurately represented by a Lorentzian distribution of the form

$$S_0(K,\omega) = N \frac{\gamma}{2\pi\hbar} \{((\omega-\omega_0)^2+(\gamma/2)^2)^{-1} - ((\omega+\omega_0)^2+(\gamma/2)^2)^{-1}\}. \qquad (3.1)$$

We can insert this expression into the Kramers-Kronig relation (2.26) and obtain the approximation

$$P_0(K,\omega) = \frac{N}{\hbar} \left\{ \frac{\omega_0-\omega}{(\omega-\omega_0)^2+(\gamma/2)^2} + \frac{\omega_0+\omega}{(\omega+\omega_0)^2+(\gamma/2)^2} \right\} \qquad (3.2)$$

for the field-free polarization function. The RPA response (2.14) for separable interactions is now also completely determined by these two analytic expressions, and using the parameters N=23.0, $\hbar\omega_0$ = 9.4 MeV, and $\hbar\gamma/2$= 13.6 MeV, all three response functions shown in Fig. 1 are quite well reproduced.

3.3 K-dependent Response.

We shall now examine the RPA response for non-zero momentum transfers along the surface. This is illustrated in Fig. 4 by contour plots. The results were obtained with a vanishing damping width Δ in the field-free Green's function and using separable residual interactions for the collective response. For the isoscalar mode we included the effect of a finite range Yukawa interaction via the K-dependent coupling constant (2.20). We used a realistic value of 1 fm for the range of this interaction.

A number of qualitative features of the response functions shown in Fig. 4 may be noted. First the divergence of the isoscalar response is quite weak, disappearing when K=0. For a fixed value of K the response has a peak

whose position increases with increasing K. This is what one would expect from the infinite Fermi gas model. The peak of the isoscalar response occurs at lower excitation energies than in the free response, whereas the peak of the isovector response is pushed towards higher excitations.

The main behavior of the free response shown in Fig. 4 can be reproduced by the Lorentzian approximation (3.1) using the K-dependent parameters

$$\begin{aligned} \hbar\omega_0(K) &= 9.4 + 0.64 \frac{\hbar^2K^2}{2m} \text{ MeV}, \\ \frac{1}{2}\hbar\gamma(K) &= 13.6 + 0.93 \frac{\hbar^2K^2}{2m} \text{ MeV}, \\ N(K) &= \frac{1}{2}\hbar\gamma(K)\ 1.69\ \{1 - 0.176\ K^2\}. \end{aligned} \qquad (3.3)$$

This parametrization of the free response can also be used to determine the RPA response (2.14) for separable interactions, as discussed in the previous section. The result obtained in this way for the isoscalar response is also shown in Fig. 4 and compares quite well with the numerical calculation.

The effects of Pauli blocking and residual interactions are illustrated in Fig. 5, where we show the K-dependence of the total response, integrated over all excitation energies. It has been normalized to the direct sum (2.25), obtained from the direct response (2.22), which contains all transitions including those that are forbidden by the Pauli principle. The Pauli blocking is seen to reduce the total free response considerably for small values of K. We show two results for the isoscalar response, one with a zero range interaction along the surface, and one with the finite range of 1 fm. The range of the interaction is seen to have a very significant effect on the total isoscalar response. The total response is divergent for K=0 in both cases. It is always enhanced compared to the total free response, whereas the total isovector response is reduced. For large values of K the effects of Pauli blocking and residual interactions are seen to diminish.

The enhancement of the total collective response over the total free response has been related to a modification of the ground state density due to the residual interactions [8]. We shall here adopt a similar model and give the final results for slab geometry without performing a detailed derivation. The particle density in the interacting ground state $\rho_I(z)$ is related to the Hartree-Fock ground state density $\rho_o(z)$ by the Gaussian folding

$$\rho_I(z) = (2\pi\Delta o^2)^{-1/2} \int dz' \exp(-\frac{(z-z')^2}{2\Delta o^2}) \rho_o(z'), \qquad (3.4)$$

c.f. ref. [8]. This result is based on a harmonic approximation for all collective degrees of freedom. For slab geometry we find that the standard deviation of the Gaussian is determined by

$$\Delta o^2 = \{2\pi \int dz\ \rho_o(z)\ V''(z)\}^{-2}$$

$$\sum_{T,S} \int d\vec{K} \int_o^\infty d\omega \{S_{T,S}(K,\omega) - S_o(K,\omega)\}, \qquad (3.5)$$

where the sum is over all spin and isospin channels. Note that the contributions from channels with repulsive interactions are negative, since the total response is reduced compared to the total free response. The quantity Δo is therefore quite sensitive to the choice of the residual interactions.

From the total isoscalar and isovector responses shown in Fig. 5 we obtain the value $\Delta o \approx 0.5$ fm using the isoscalar interaction with the finite range of 1 fm along the surface. Using instead the zero range interaction we obtain a much larger value, $\Delta o \approx 1$ fm. Contributions from the spin channels with repulsive interactions will reduce this value further. We do not want to put too much emphasis on the absolute numerical value of Δo, since it is a sensitive quantity. Let us mention that from the study of spherical nuclei

[8] a value of $\Delta o \approx 0.3$ fm was obtained for ^{208}Pb. In section 5 we will relate the polarization of the slab to its surface tension. We shall see that a reasonable value for the surface tension is only obtained with a finite range interaction, supporting the smaller value of Δo mentioned above.

4. Fermi Gas Approximation.

The main features of the free and the isovector surface response discussed in section 3.1 are also observed for the response of an infinite Fermi gas. The translational invariance of the infinite system makes it easy to solve the RPA equation, as shown in Appendix B. It is of interest to examine how close the responses agree, because of the convenience of a simple solution. The main question is the choice of parameters for the infinite system that will be compared. One approximation that is commonly made for describing surface properties is the local Fermi gas approximation [9]. The idea is to replace any operator depending on coordinates by the corresponding operator for an infinite Fermi gas with a density evaluated at the average coordinate position. We will discuss the local Fermi gas approximation below. An even simpler approximation is to evaluate the operator at a uniform density chosen to be an appropriate average density in the surface region. We may choose this density by demanding that the EWSR for the infinite medium matches that of the inhomogenous system. For the slab response discussed in section 3.1 the equivalent matter density is $\rho_0 = 0.058\ fm^{-3}$ for K=0. We compare the free response of this system with the free surface response (dashed curve) in Fig. 6. The agreement is quite good, with a reasonable shape and peak that deviates by about 10%. If this free response is used to calculate the RPA response with a separable interaction, the interacting response would come out well because all that is required in the separable model is integrals over the free response, as discussed in section 3.2. The separable isovector response is shown in Fig. 6 also, and may be compared with the surface isovector response from Fig. 1. The shapes are nearly identical, but the height of the peak for the infinite Fermi gas is about 20% too low.

It is also of interest to examine the response for the δ-function interaction (2.18), which is much better justified than the separable interaction for the isovector mode. An interesting feature of the isovector response of an infinite Fermi gas is the existence of a collective branch outside the region of the free response in the (k,ω) plane (see appendix B). This branch is analogous to zero sound, which occurs when the interaction is repulsive. The mode is undamped in the RPA, i.e. the induced density does not decay at large distances. Some effect of this behavior may be seen in Fig. 3. In the present example the branch merges with the free response at excitation energies above 12 MeV. Its contribution to the total isovector response is indicated by the shaded area in Fig. 6.

Note that the isovector response for the δ-function interaction is somewhat reduced as compared to the result for the separable interaction. This behavior was also found for the surface response in Fig. 2. We conclude that the Fermi gas model is a useful approximation for the free response and the interacting response when the interaction is repulsive. Moreover, the calculation of the RPA response for a δ-function interaction is almost trivial for an infinite Fermi gas, whereas it requires the inversion of a matrix for an inhomogenous system.

We now turn to the more elaborate local Fermi gas approximation. We first note that it is sufficient to reproduce the behavior of the free response, for models with separable interactions. We will therefore example the free Green's function, which we calculate as

$$G_{FGM}(z,z',K,\omega) = \frac{4}{2\pi}\int dk_z\ G_0(\rho_0(Z),k,\omega)\ \exp(ik_z(z-z')), \qquad (4.1)$$

Here $k=\sqrt{K^2+k_z^2}$, and G_0 is the field-free Greens function given in Appendix B for a Fermi gas of some density $\rho_0(Z)$. The density is evaluated at a point Z

which we choose to be the midpoint of the coordinates, $Z=(z+z')/2$. Using the integration variables Z and $\xi=z-z'$, the associated response due to the external field (2.7) is given by

$$S_{FGM}(K,\omega) = \frac{4}{2\pi^2}\int dZ \int dk_z \; \mathrm{Im}\{G_o(\rho_o(Z),k,\omega)\}\; \chi(k_z,Z), \qquad (4.2)$$

where

$$\chi(k_z,Z) = \int d\xi \; V'(Z+\xi/2)\; \exp(ik_z\xi)\; V'(Z-\xi/2). \qquad (4.3)$$

The energy-weighted sum rule for this response function can easily be obtained from the sum rule (B.6), and one finds that

$$\hbar^2 \int_0^\infty d\omega \; \omega S_{FGM}(K,\omega) =$$

$$\frac{\hbar^2}{2m}\int dz \; \rho_o(z)\{(V''(z))^2 + K^2(V'(z))^2 - \frac{1}{4}\frac{\partial^2}{\partial z^2}(V'(z))^2\}. \qquad (4.4)$$

The first and the second term in the parenthesis constitute the exact EWSR (2.24) for the slab response. Because of the third term, the local Fermi gas approximation falls short of the exact EWSR by 23% at K=0. Note that the third term would become negligible for slowly varying densities. For high K, the sum is dominated by the second term and one would expect a better agreement with the exact response. This is confirmed by the comparison shown in Fig. 7. For K=0 there is a large discrepancy with the local Fermi gas approximation underestimating the surface response by 30% at the peak position. For K>1 fm^{-1} the agreement is much better. In contrast, the constant density Fermi gas model discussed above is in excellent agreement for K=0 but would require readjustments of the constant density for different K values.

5. Static Polarization.

If a static external field is applied to a liquid at its surface, the surface will distort to achieve a stable state of minimum energy. In Hartree-Fock theory, the distortion can be determined from the RPA response to the external field at $\omega=0$. We can apply the response theory of sections 2 and 3, if we choose the field to have the form

$$-V'(z)\cos(Kx). \qquad (5.1)$$

The change in density is then given by Eq. (2.13). The associated polarization, defined in (2.9), is

$$P_{RPA}(K) = \int dz \; V'(z)\; \delta\rho_{RPA}(z,K) = \frac{P_o(K)}{1+\kappa(K)P_o(K)}, \qquad (5.2)$$

where $P_o(K)$ is the static polarization function of the Hartree-Fock ground state.

Classically, the amplitude of the distortion is determined by the surface tension σ of the liquid. Let us define an amplitude β for the distortion,

$$\delta\rho_{Class}(z,x) = -\beta\,\rho_o'(z)\cos(Kx). \qquad (5.3)$$

The average energy per unit area in the external field (5.1) is

$$E = \frac{1}{4}(\beta K)^2\,\sigma + \frac{1}{2}\beta\int dz\;\rho_o'(z)\;V'(z). \qquad (5.4)$$

Minimizing this energy produces the classical formula for the static polarization function

$$P_{Class}(K) = \int dz \; V'(z)\; \delta\rho_{Class}(z,K) = \frac{(P_o(0))^2}{K^2\sigma}, \qquad (5.5)$$

where $P_o(0)$ is the static field-free polarization (2.17) for K=0. Notice that the classical expression diverges quadratically at K=0. The same quadratic divergence occurs in RPA theory. This follows simply from the self-consistency condition used to derive the coupling constant (2.15) for K=0, and the fact that $P_o(K)$ is an even function of K. Equating Eqs. (5.5)

and (5.2), we can derive a relation for the effective surface tension of the RPA model,

$$\sigma_{eff} = \frac{(P_0(0))^2}{K^2} \frac{1+\kappa(K)P_0(K)}{P_0(K)} . \qquad (5.6)$$

In Appendix C the static polarization function $P_0(K)$ for the non-interacting ground state is expanded to second order in K. Furthermore, expanding the coupling constant (2.20), we obtain the following expression in the long wave length limit

$$\sigma_{eff} = 2\Delta T + \frac{1}{2} a_r^2 P_0(0). \qquad (5.7)$$

In the first term ΔT is the difference of the ground state kinetic energy (per unit area) in the z-direction perpendicular to the surface and in a direction parallel to the surface. The second term arises from the finite range a_r of the isoscalar interaction along the surface. The result (5.7), based on the relation between the surface tension and the static polarization, is equivalent to the expression derived by Feibelman [4], who treated the quantum pressure rather than the polarization at the surface.

For our parametrization of the slab we find that $2\Delta T = 0.25$ MeV/fm^2. A reasonable range for a Yukawa interaction is 1 fm, for which (5.7) gives a contribution to the surface tension of 0.78 MeV/fm^2. Thus the total surface tension is about 1 MeV/fm^2 in good agreement with the empirical value. Since the finite range of the interaction is responsible for most of the surface tension, it is important to include the finite range in calculating properties related to the surface tension. One of these properties is the surface fluctuation discussed in section 3.3, which came out much too large when this range was set to zero.

6. Applications to Finite Nuclei.

In this section we will apply the theory to finite spherical nuclei and compare with the empirical nuclear response. The finite geometry implies that the modes are discrete rather than continuous functions of wave number and frequency. So we expect that only the gross features of the nuclear response are reproduced by the semi-infinite theory. Sharp structures of the response such as giant resonances will not be reproduced. The appropriate fields for describing spherical nuclei have an angular dependence given by spherical harmonics. The connection between these fields and the wave number in a semi-infinite geometry can be made via the asymptotic expansion for the Legendre function,

$$P_\ell(\cos\theta) \approx J_0(\ell\theta) \approx J_0(K\rho),$$

where ρ is an arc length along the surface of a sphere of radius R and $K=\ell/R$.

One averaged property of nuclei that is rather stable is the fraction of the energy-weighted sum rule at low excitation. Only the scalar fields have significant strength at low excitation, and typically there is about 10-15% of the sum rule concentrated in a state at excitation energy below 5 MeV. The semi-infinite slab has a strong response only for scalar fields as well, with the response diverging at zero frequency and wave number. As discussed in section 3, the EWSR is finite even when the response itself diverges; the sum rule fraction below 5 MeV is 13%, in remarkable agreement with the finite nucleus systematics. One can conclude from this that the low frequency response of nuclei is dictated in overall strength by the nuclear matter surface dynamics. The specific shell structures are only responsible for the details of the effective restoring force in the surface deformation modes.

To obtain a more global perspective of the nuclear surface response we may examine inelastic scattering of strongly absorbed projectiles. At high energies, the geometry of the projectile-target interaction are simple enough to make a direct connection between scattering angle and wave number of the excitation field. The energy loss of the projectile directly measures the excitation energy of the target. We shall now apply the RPA response to (p,p') data at 800 and 319 MeV. We connect the semi-infinite response to the scattering on spherical nuclei using the method of [10]. They calculate the response of the slab using the external field

$$U(\vec{r}) = U_o(z)\ \exp(i\vec{q}_p\vec{r}_p), \tag{6.1}$$

where

$$U_o(z) = \exp(iq_z z)\ \{1 + \exp((z_o-z)/a_o)\}^{-1/2}$$

and $\vec{q}=(\vec{q}_p,q_z)$ represents the momentum transfer. The Fermi-function, with parameters a_o and z_o, simulates the functional form of the absorption one would have in a spherical nucleus according to Glauber theory. The associated free response of the slab is

$$S_o(q,\omega) = \frac{1}{\pi}\ \mathrm{Im}\{\int dz \int dz'\ U_o(z)^*\ G_o(z,z',q_p,\omega)\ U_o(z')\}. \tag{6.2}$$

There is no simple expression for the non-energy weighted sum of this response due to the presence of the Pauli-blocking in the Green's function. However, if we neglect the Pauli-blocking for a moment, the direct sum rule (2.25) would apply, viz.

$$S_{norm} = \int dz\ \rho_o(z)\ \{1+\exp((z_o-z)/a_o)\}^{-1} \tag{6.3}$$

In ref. [10] the response is normalized to this sum, and the single-scattering cross section is calculated from the factorized formula

$$\frac{d^2\sigma}{d\Omega dE} = \left\{\frac{d\sigma}{d\Omega}\right\}^{el}_{NN}\ N_{eff}\ S_o(q,\omega) / S_{norm}, \tag{6.4}$$

which contains the elastic nucleon-nucleon cross section, the normalized response, and an effective number of target nucleons N_{eff}. The latter quantity is adjusted so that the total single-scattering cross section is consistent with Glauber Theory (see ref. [10] for details).

Note that the calculation of the field-free Green's function now involves one extra numerical integration over the orientation of the momentum transfer $\hbar\vec{q}$ in the plane perpendicular to the beam direction. Since the calculation of the collective respose, using a realistic residual interaction, was already quite time-consuming for K=0, and since the separable interactions yielded almost the same results, we shall in the following only use separable interactions.

For each spin-isospin channel (S,T) we calculate the collective response $S_{T,S}(q,\omega)$ from the RPA Greens function (2.12), using the scattering operator (6.1) as the external field. The coupling strengths for the separable residual interactions in the different channels are given in section 2.4. The associated elastic scattering cross sections, $(d\sigma/d\Omega)^{el}_{T,S}$, can be extracted from the general parametrization of the proton-proton the and proton-neutron scattering amplitudes [11], as shown in Appendix D. Similar to Eq. (6.4) we can then calculate the inelastic proton-nucleus cross sections for exciting the different spin-isospin modes in the target nucleus from the expression

$$\left\{\frac{d^2\sigma}{d\Omega dE}\right\}_{T,S} = \left\{\frac{d\sigma}{d\Omega}\right\}^{el}_{T,S}\ N_{eff}\ S_{T,S}(q,\omega) / S_{norm}. \tag{6.5}$$

The total inelastic cross section, summed over all spin-isospin channels, is shown in Fig. 8 for 800 MeV protons scattered on a ^{116}Sn target. The cross section obtained from the free response is also shown. Note the enhancement of the total cross section compared to the free

response for low excitation energies. It is mainly due to the isoscalar response, which in fact dominates with more than 70 % over the entire energy range shown in the figure. The measured cross section [12] shows an even larger enhancement for low excitation energies, with structures that are not contained in the slab response. These structures are the well known giant resonances, which are specific properties of the finite geometry of the nucleus.

Recent measurements of spin-flip cross sections [13] provide new information on the residual interaction in the S=1 excitation channels. The elastic cross section for a spin-flip of the incoming proton is given in Appendix D, and the corresponding inelastic cross section can be determined from the expression

$$\left\{ \frac{d^2\sigma}{d\Omega dE} \right\}_{spf} = \sum_{T=0,1} \left\{ \frac{d\sigma}{d\Omega} \right\}^{el}_{T,spf} N_{eff} \, S_{T,S=1}(q,\omega) \; / \; S_{norm}, \qquad (6.6)$$

summing over the S=1 isospin channels. The predictions of the slab model is compared with experimental results in Fig. 9 for 319 MeV protons on a ^{90}Zr target. Note the shift in the position of the maximum compared to the free response. This shift originates from the residual interaction in the (T=1,S=1) excitation channel which dominates the spin-flip cross section by about 70%. Within the model there are no free parameters, so the absolute agreement is a success both for the theory of the response and the impulse approximation theory of the projectile-target interaction. We also predict that the spin-flip cross section peak is just the region of the current data.

7. Conclusions.

The present investigation of the surface response of a semi-infinite Fermi liquid, based on the Random Phase Approximation, illustrates some basic features of the surface response of self-bound, interacting many-body systems. It is especially relevant for the quasi-elastic scattering on heavy nuclei of high-energy probes that are strongly absorbed in the nuclear interior.

The residual interaction in the isoscalar channel is partly determined by self-consistency, and partly from the range of the interaction in directions parallel to the surface. Phenomenological interactions have been used for other spin-isospin channels. The isoscalar response of the semi-infinite system exhibits a large enhancement at low excitation energies compared to the free-response, with a significant fraction of the energy-weighted sum rule that is typical for the response of finite nuclei.

Separable residual interactions lead to quite reasonable response functions, compared to more realistic interactions. The separable interaction has the advantage that the associated collective response can be determined directly from the coupling constant and the free response, which in the present study is quite well represented by Lorentzian distributions.

A local Fermi gas model, based on the Green's function of an infinite Fermi gas, but suitably modified to describe the response of an inhomogenous system, is rather successful for large momentum transfers along the surface. For zero momentum transfer, however, the model is unreliable to describe the surface response of the semi-infinite Fermi gas. In this case the much simpler model of an infinite Fermi gas is more useful. In this model the isovector and the free response simulate the surface response quite well,

provided the density of the infinite system is chosen so that the energy-weighted sum of the surface response is reproduced.

The finite range of the isoscalar residual interaction parallel to the surface has some very significant consequences. In our formulation it enters into the separable interaction through an effective coupling constant that depends on the momentum transfer along the surface. It leads to a reduction of the interaction for a non-zero momentum transfer, compared to the case of a zero-range interaction. Fluctuations in the surface density of the interacting ground state are consequently also reduced. Moreover, the effective surface tension, extracted from the static isoscalar polarization, is about 1 MeV/fm^2 and it is dominated by the contribution from the finite range of the interaction along the surface, whereas the contribution from the kinetic energy is surprisingly small.

The predominance of the isoscalar response at low excitations can explain the main features of quasi-elastic scattering data for high-energy protons. The response in the spin channels is also well reproduced, when a reasonable strength of the interaction is included in the RPA calculation. The detailed structures of giant resonances, however, are not directly seen in the response of the semi-infinite system. If the aim of the theory is to describe the overall behavior of the response, and not specific resonant features, the semi-infinite slab model is very successful.

Acknowledgments.

Valuable discussions with J.W.Negele, O.Scholten and P.J.Siemens are gartefully acknowledged. We also acknowledge support by the National Science Foundation under Grant PHY-80-17605.

References.

1. D.M.Newns, Phys. Rev. B8, 3304 (1970).
2. P.Feibelman, Phys. Rev. B12, 1319 (1975).
3. R.G.Barrera and A.Bagchi, Phys. Rev. B20, 3186 (1979).
4. P.Feibelman, Ann. Phys. 48, 369 (1968).
5. G.F.Bertsch, D.Cha and H.Toki, Phys.Rev. C24, 533 (1981).
6. G.F.Bertsch, Prog. of Theor. Physics, Nos. 74-75, 115 (1983).
7. G.F.Bertsch and S.F.Tsai, Phys. Rep. 18C, 126 (1975).
8. H.Esbensen and G.F.Bertsch, Phys.Rev. C28, 355 (1983).
9. T.Izumoto, M.Ichimura, C.M.Ko and P.J.Siemens, Phys. Lett. 112B, 315 (1982).
10. G.F.Bertsch and O.Scholten, Phys.Rev C25, 804 (1982).
11. S.J.Wallace, Adv. in Nucl. Phys., Vol 12, 135 (1981).
12. J.M.Moss, et al., Phys. Rev. Lett. 48, 789 (1982).
13. S.K.Nanda, et al., Phys. Rev. Lett. 51, 1526 (1983).
14. C.Mahaux and H.A.Weidenmüller, "Shell model approach to nuclear reactions", p.11, North-Holland, Amsterdam, 1969.
15. J.Lindhard, Mat.Fys.Medd.Dan.Vid.Selsk. 28, no. 8 (1954).

Appendix A: Free Response.

The initial states of a semi-infinite slab, with energies $\epsilon_i = (\hbar k_i)^2/2m$, have the form

$$\phi_i(\vec{r}) = \phi_i(z)\exp(i\vec{k}_i\vec{r}_p). \tag{A.1}$$

The z-dependent part of these wave functions are solutions to the Schrödinger equation

$$H_{0z}\phi_i(z) = \left[-\frac{\hbar^2}{2m}\frac{\partial^2}{\partial z^2} + V(z)\right]\phi_i(z) = \epsilon_{iz}\phi_i(z), \tag{A.2}$$

where $\epsilon_{iz}=(\hbar k_{iz})^2/2m$. They can be normalized to have the asymptotic behavior

$$\phi_i(z) \to \sqrt{2}\cos(k_{iz}z + \theta_i), \text{ for } z \to -\infty, \tag{A.3}$$

so that the spatial average value of $|\phi_i|^2$ is unity in the interior of the slab. The unperturbed density of the slab is

$$\rho_o(z) = \frac{4}{(2\pi)^3}\int_F d\vec{k}_i\ |\phi_i(z)|^2. \tag{A.4}$$

The subscript (F) on the integral indicates that all states below the Fermi surface are included in the integration, and the factor of 4 accounts for spin and isospin degeneracy. The Fermi momentum is related to the density in the interior of the slab by $2k_F^3/(3\pi^2) = \rho_o(-\infty) = 0.16\ \text{fm}^{-3}$.

We define the direct field-free Green's function for the slab as follows

$$G_o^D(\vec{r},\vec{r}',\omega) = \frac{4}{(2\pi)^3}\int_F d\vec{k}_i\ \phi_i^*(\vec{r})\langle\vec{r}|(H_o-\epsilon_i-\hbar\omega-i\Delta)^{-1}|\vec{r}'\rangle\phi_i(\vec{r}'). \tag{A.5}$$

The quantity Δ is greater than zero to ensure causality. It is usually considered as vanishingly small, but in some cases discussed in section 3 we choose a finite value for Δ in order to improve the numerical convergence. The retarded field-free Green's function used in Eq. (2.4) is

$$G_o(\vec{r},\vec{r}',\omega) = (G_o^D(\vec{r},\vec{r}',\omega) + (G_o^D(\vec{r},\vec{r}',-\omega))^*. \tag{A.6}$$

The induced density due to an external perturbation $U(\vec{r})$ that is oscillating in time with the frequency ω, is given by

$$\delta\rho_o(\vec{r},\omega) = -\int d\vec{r}'\ G_o(\vec{r},\vec{r}',\omega)\ U(\vec{r}'). \tag{A.7}$$

Our system is translationally invariant in the two directions parallel to the surface of the slab. We can therefore Fourier transform with respect to the x-y coordinates along the surface, and obtain the equation

$$\delta\rho_o(z,K,\omega) = -\int dz'\ G_o(z,z',K,\omega)\ U(K,z'). \tag{A.8}$$

Here $G_o(z,z',K,\omega)$ is constructed, as in Eq. (A.6), from the direct Green's function

$$G_o^D(z,z',K,\omega) = \frac{4}{(2\pi)^3}\int_F d\vec{k}_i\ \phi_i(z)\ \phi_i(z')$$

$$\langle z|(H_{0z} + \frac{\hbar^2}{2m}(K^2+2\vec{K}\vec{k}_i) - \epsilon_{iz} - \hbar\omega - i\Delta)^{-1}|z'\rangle, \tag{A.9}$$

which is seen to be independent of the orientation of $\vec{K}$. We calculate the latter single-particle Green's function using the exact representation [14]

$$\langle z|(H_{0z}-E-i\Delta)^{-1}|z'\rangle = -\frac{2m}{\hbar^2 W}u(z_<)v(z_>). \tag{A.10}$$

The functions u and v are solutions to the equation $H_{0z}\phi = (E+i\Delta)\phi$, obeying the boundary conditions

$$u(z) \to \exp(-ikz), \text{ for } z \to -\infty, \tag{A.11}$$

where $k = \sqrt{2m(E+i\Delta)}/\hbar$, and

$$v(z) \to \exp(ikz), \text{ for } z \to \infty, \tag{A.12}$$

where $k = \sqrt{2m(E+i\Delta-V_o)}/\hbar$. The quantity W is the Wronskian of the two solutions: $W = uv'-vu'$.

Appendix B: Fermi Gas Model.

For an infinite Fermi gas of nuclear matter the field-free Green's function is

$$G_o(\vec{r},\vec{r}',\omega) = (2\pi)^{-3} \int d\vec{k}\; G_o(k,\omega)\; \exp(i\vec{k}(\vec{r}-\vec{r}')), \tag{B.1}$$

where

$$G_o(k,\omega) = \frac{4}{(2\pi)^3} \int_F d\vec{k}_1 \left\{(\varepsilon_{f1}-\hbar\omega-i\eta)^{-1} + (\varepsilon_{f1}+\hbar\omega+i\eta)^{-1}\right\}, \tag{B.2}$$

and $\varepsilon_{f1} = \frac{\hbar^2}{2m}(k^2+2\vec{k}\vec{k}_1)$ and $k_F^3 = \frac{3\pi^2}{2}\rho_o$. The factor 4 takes care of spin and isospin degeneracy. This function can be expressed in terms of the Lindhard functions [15] as follows

$$G_o(k,\omega) = \frac{3\rho_o}{2\varepsilon_F}\left\{f_1(\xi,u)+if_2(\xi,u)\right\}, \tag{B.3}$$

where $\xi = k/2k_F$ and $u = \omega/kv_F$. For a planar field $V_{ext}(z)$ the induced density $\delta\rho_o(z,\omega)$ has the Fourier transform

$$\delta\rho_o(k,\omega) = -\, G_o(k,\omega)\; V_{ext}(k) \tag{B.4}$$

and the free response is

$$S_o(\omega) = \frac{1}{2\pi^2}\int_{-\infty}^{+\infty} dk\; \mathrm{Im}\{G_o(k,\omega)\}\; |V_{ext}(k)|^2. \tag{B.5}$$

The energy-weighted sum rule (2.24) can be expressed in a more detailed form for each Fourier component of the external field as follows

$$\frac{\hbar^2}{\pi}\int_0^\infty d\omega\; \omega \mathrm{Im}\{G(k,\omega)\} = \frac{\hbar^2k^2}{2m}\rho_o. \tag{B.6}$$

The self-consistent equation (2.4) can easily be solved in Fourier space, if the residual interaction is of the folding type

$$\mathcal{V}(\vec{r}-\vec{r}') = (2\pi)^{-3}\int d\vec{k}\,\mathcal{V}(k)\; \exp(i\vec{k}(\vec{r}-\vec{r}')), \tag{B.7}$$

i.e. translationally invariant. The equation is then

$$\delta\rho(k,\omega) = -\, G_o(k,\omega)\left\{V_{ext}(k) + \mathcal{V}(k)\delta\rho(k,\omega)\right\}, \tag{B.8}$$

and the imaginary part of the RPA Green's function is

$$\mathrm{Im}\{G_{RPA}(k,\omega)\} = \frac{3\rho_o}{2\varepsilon_F}\,\frac{f_2}{(1+\chi f_1)^2+(\chi f_2)^2} \tag{B.9}$$

where $\chi = 3\rho_o\mathcal{V}(k)/(2\varepsilon_F)$. This function also obeys the sum rule (B.6). The sum may consist of two contributions, viz. one from the single-scattering region ($f_2 \neq 0$) and one from a collective mode ($f_2 = 0$ and $1+\chi f_1 = 0$). The contribution from the collective mode is indicated in Fig. 6 for the isovector response of a Fermi gas.

Appendix C: Static Properties.

In this appendix we shall expand the static polarization to second order in the momentum transfer along the surface, for the purpose of relating it to the surface tension in section 5. The algebraic manipulations are similar to those in ref. [4], where the quantal pressure was related to the surface tension. The static properties of the non-interacting ground state of a semi-infinite slab is determined by the Green's function (c.f. Eqs. (A.6) and (A.9))

$$G_o(z,z',K,0) = \frac{4}{(2\pi)^3} \int_F d\vec{k}_i \; 2\phi_i(z)\langle z|(H_{oz}+\Delta E_i-\epsilon_{iz})^{-1}|z'\rangle\phi_i(z'), \quad (C.1)$$

where $$\Delta E_i = \frac{\hbar^2}{2m}\left[K^2+ 2Kk_{ix}\right] \quad (C.2)$$

is the energy loss associated with the momentum transfer $\hbar K$ in the x-direction parallel to the surface. This function is a real function.

We first determine the induced density for a static and uniform displacement of the surface. For a small displacement δz the external field on the slab is $-V'(z)\delta z$, and the the induced density (in units of δz) becomes

$$\delta\rho_o(z) = \int dz' \; G_o(z,z',0,0)\; V'(z'). \quad (C.3)$$

We can evaluate this expression using the commutation relation

$$\left[H_{oz}, \frac{\partial}{\partial z}\right] = -V'(z) \quad (C.4)$$

i.e.

$$(H_{oz}-\epsilon_{iz})^{-1}V'(z)\phi_i(z) = -\phi_i'(z). \quad (C.5)$$

From Eqs. (C.1) and (C.3) we thus obtain

$$\delta\rho_o(z) = \frac{4}{(2\pi)^3} \int_F d\vec{k}_i \; \left[-2\phi_i(z)\phi_i'(z)\right] = -\rho_o'(z), \quad (C.6)$$

which is the result stated in Eq. (2.16).

We shall now expand the static polarization function

$$P_o(K) = \int dz \int dz' \; V'(z)\; G_o(z,z',K,0)\; V'(z') \quad (C.7)$$

to second order in K. We therefore expand the inverse operator in Eq. (C.1) to second order in ΔE_i. Since we shall perform an integration over the Fermi sphere, we can effectively use the approximation

$$(H_{oz}+\Delta E_i-\epsilon_{iz})^{-1} \approx (H_{oz}-\epsilon_{iz})^{-1}$$

$$- \frac{\hbar^2K^2}{2m}\left\{(H_{oz}-\epsilon_{iz})^{-2} - 2\,\frac{\hbar^2}{m}\,k_{ix}^2(H_{oz}-\epsilon_{iz})^{-3}\right\}. \quad (C.8)$$

The first term yields the simple result

$$P_o(K=0) = \int dz\; V'(z)\;\delta\rho_o(z) = \int dz\; \rho_o(z)\; V''(z). \quad (C.9)$$

Eq. (C.5) can also be used to evaluate the contribution from the second term. To evaluate the third term we make use the commutation relation

$$\left[H_{oz}, z\right] = -\frac{\hbar^2}{m}\frac{\partial}{\partial z}. \quad (C.10)$$

From this relation and Eq. (C.5) we find that

$$(H_{oz}-\epsilon_{iz})^{-2}V'(z)\phi_i(z) = \frac{m}{\hbar^2}\,z\phi_i(z). \quad (C.11)$$

The static polarization function to second order in K is therefore

$$P_o(K) = P_o(K=0) - 2\,K^2\,\Delta T, \quad (C.12)$$

where

$$\Delta T = \int dz\,\frac{4}{(2\pi)^3}\int_F d\vec{k}_i\,\frac{\hbar^2}{2m}\left\{(\phi_i'(z))^2 + k_{ix}^2 2z\phi_i(z)\phi_i'(z)\right\}. \quad (C.13)$$

For a finite system we perform a partial integration so that $2z\phi_i(z)\phi_i'(z)$ is replaced by $-(\phi_i(z))^2$. The quantity ΔT is then the difference between the kinetic energy (per unit area) in the z-direction perpendicular to the surface and the kinetic energy in a direction parallel to the surface.

Appendix D: Elastic Scattering.

The general parametrization of the elastic nucleon-nucleon scattering amplitude $f(\vec{q})$ has the following form in the center of mass system [11]

$$(2ik_{CM})^{-1} f(\vec{q}) = A + iqC(\vec{\sigma}_1\vec{n}+\vec{\sigma}_2\vec{n}) + B\vec{\sigma}_1\vec{\sigma}_2 + D(\vec{\sigma}_1\vec{q})(\vec{\sigma}_2\vec{q}) + E\sigma_{1z}\sigma_{2z}, \quad (D.1)$$

where $\vec{q}$ represents the momentum transfer. The z-axis is here along the average (initial-final) momentum direction, and $\vec{n}$ is a unit vector perpendicular to the scattering plane. From the proton-proton (pp) and the proton-neutron (pn) amplitudes, tabulated in [11], we can determine the elastic isoscalar and isovector amplitudes by

$$f_{T=0}(\vec{q}) = [f_{pp}(\vec{q}) + f_{pn}(\vec{q})]/2, \quad (D.2)$$

$$f_{T=1}(\vec{q}) = [f_{pp}(\vec{q}) - f_{pn}(\vec{q})]/2, \quad (D.3)$$

respectively. These amplitudes are again parametrized as in Eq. (D.1), with coefficients A_T through E_T. We can now construct the elastic cross sections for the different spin-isospin excitation modes of the target. For the S=0 channels one finds that

$$\left\{ \frac{d\sigma}{d\Omega} \right\}^{el}_{T,S=0} = (2k_{CM})^2 \{|A_T|^2 + q^2|C_T|^2\}, \quad (D.4)$$

and for the S=1 channels one finds

$$\left\{\frac{d\sigma}{d\Omega}\right\}^{el}_{T,S=1} = (2k_{CM})^2 \{|B_T|^2 + |B_T+q^2D_T|^2 + |B_T+E_T|^2 + q^2|C_T|^2\}. \quad (D.5)$$

Of particular interest is the cross section for a spin-flip of the incoming proton. The elastic cross section for this process is given by the expression

$$\left\{ \frac{d\sigma}{d\Omega} \right\}_{T,spf} = (2k_{CM})^2 \{|B_T+q^2D_T|^2 + |B_T+E_T|^2\}. \quad (D.6)$$

Figure Captions:

Fig. 1. Response functions for the semi-infinite slab due to the external field (2.7). The momentum transfer parallel to the surface is zero. The collective response functions are based on the separable residual interactions given in section 2.4.

Fig. 2. Response functions for the semi-infinite slab obtained with a finite damping width of Δ = 2 MeV in the field-free Green's function. The free response and the isoscalar and isovector response for separable residual interactions are shown as full drawn curves. Also shown is the isoscalar (●) and the isovector (▲) response for the δ-function interactions discussed in section 2.4.

Fig. 3. Induced densities associated with the free response and with the isoscalar and isovector response for δ-function interactions, at an excitation energy of 15 MeV. The full drawn curves represent the real part and the dashed curves are the imaginary part of the induced densities. The damping width in field-free Green's function was Δ = 2 MeV.

Fig. 4. Contour plots of the free response and the isoscalar and isovector response for separable interactions, as functions of the excitation energy and the momentum transfer MK parallel to the surface of the semi-infinite slab. For the isoscalar response the coupling strength (2.20) for a finite range of 1 fm was used. Also shown is the isoscalar response obtained, as described in Section 3.2, from a Lorentzian fit to the free response with the parameters given in Eq. (3.3).

Fig. 5. Total responses, obtained from the response functions shown in Fig. 4 by integration over all excitation energies. They are shown as functions of the momentum transfer $\hbar K$ parallel to the surface of the semi-infinite slab and have been normalized to the total direct response (2.25). For the isoscalar response the results for the zero-range separable interaction is also shown (dashed curve).

Fig. 6. Free response and isovector response of an infinite Fermi gas with a density of 0.058 fm^{-3}, due to the external field (2.7) for K=0. The free response of the semi-infinite slab is also shown (dashed curve). The isovector response is given both for the δ-function residual interaction and for the separable interaction (Sep. Int.). The dashed area below 12 MeV of excitation is the contribution from the collective isovector mode, which is similar to zero sound.

Fig. 7. The free response of the semi-infinite slab for different values of the momentum transfer $\hbar K$ parallel to the surface. The dashed curves were obtained from the local Fermi gas model described in section 4.

Fig. 8. Experimental [12] and calculated inelastic cross sections for 800 MeV protons on ^{116}Sn, at a fixed laboratory scattering angle of 5 degrees. The two calculated curves were obtained from the free response of a semi-infinite slab (dashed curve), and from the collective responses, summing (6.5) over all spin and isospin channels (full drawn).

Fig. 9. Experimental [13] and calculated inelastic cross sections for spin-flip of 319 MeV polarized protons on ^{90}Zr, at a fixed laboratory scattering angle of 3.5 degrees. The calculated results were obtained from Eq. (6.6) using the field-free response (dashed curve) and the collective responses in the S=1 spin excitation channels, respectively.

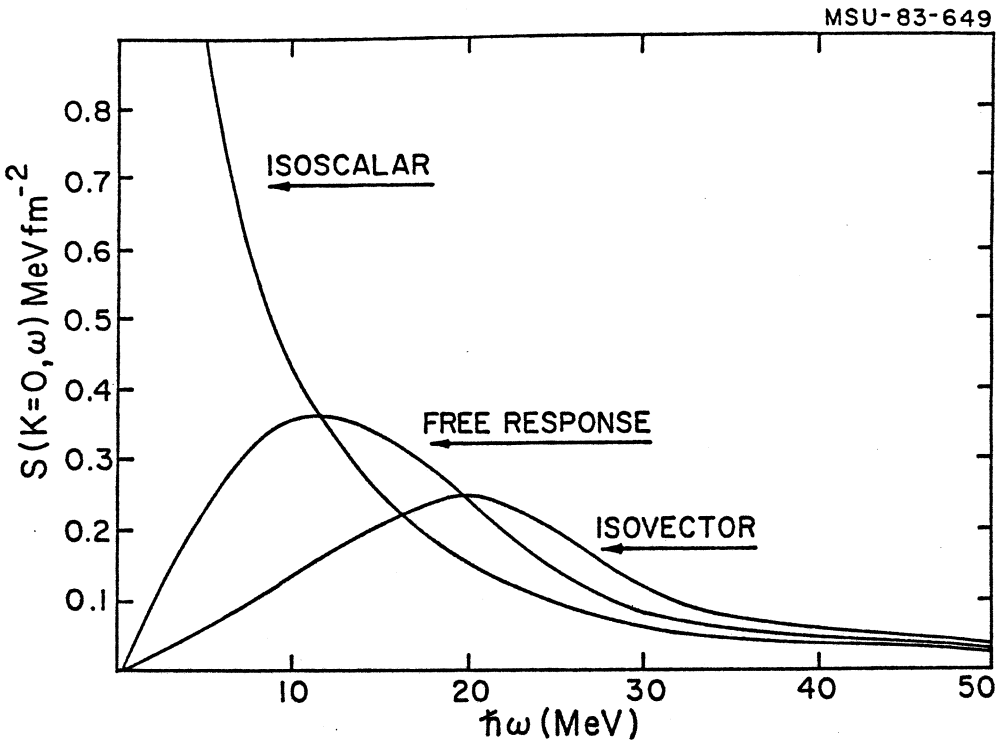

Figure 1

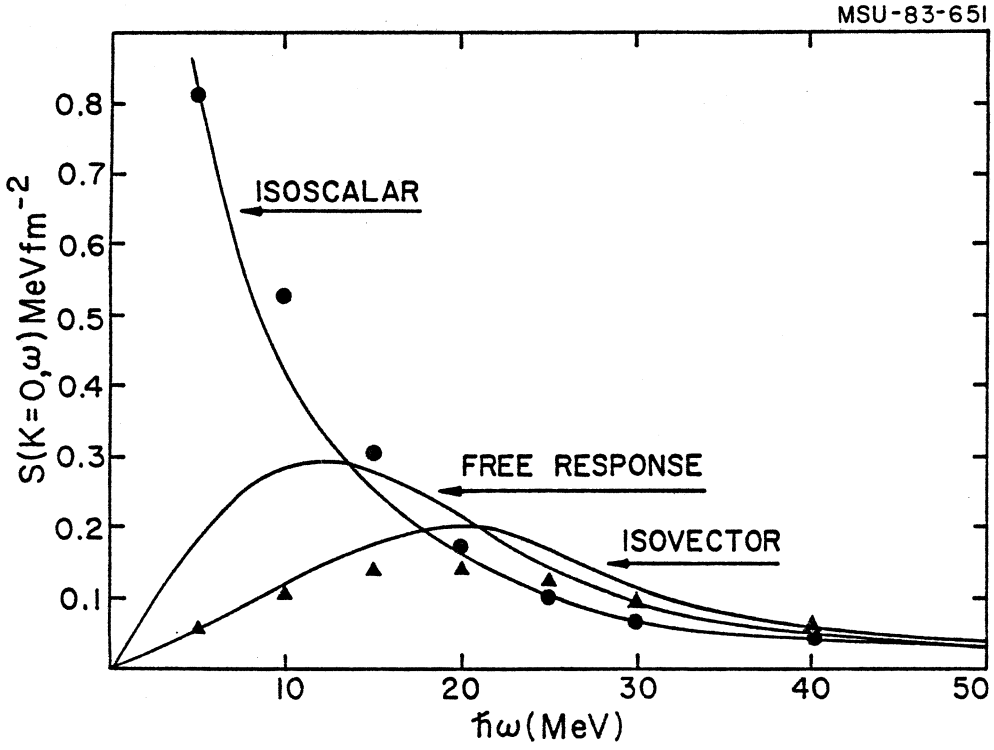

Figure 2

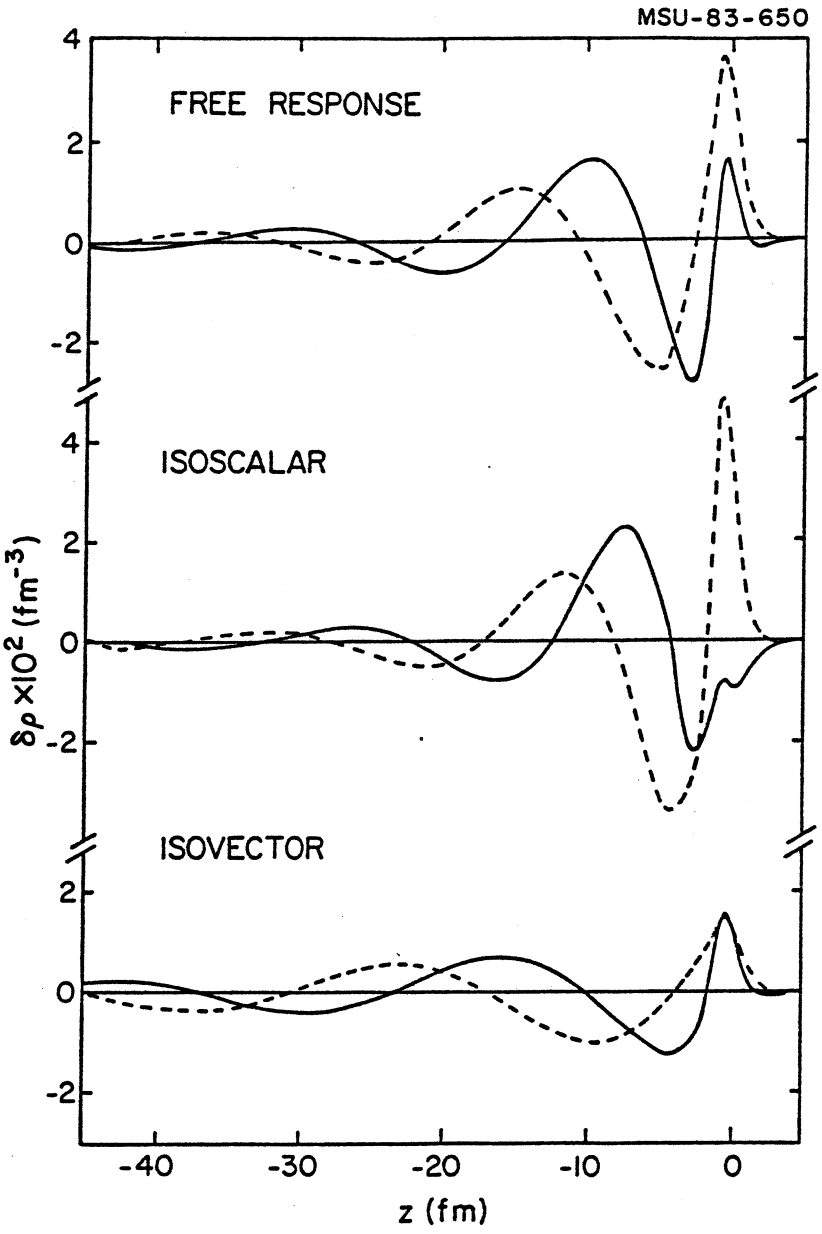
MSU-83-650
FREE RESPONSE
ISOSCALAR
ISOVECTOR
δρ X10² (fm⁻³)
z (fm)
4
2
0
-2
-40
-30
-20
-10
0

Figure 3

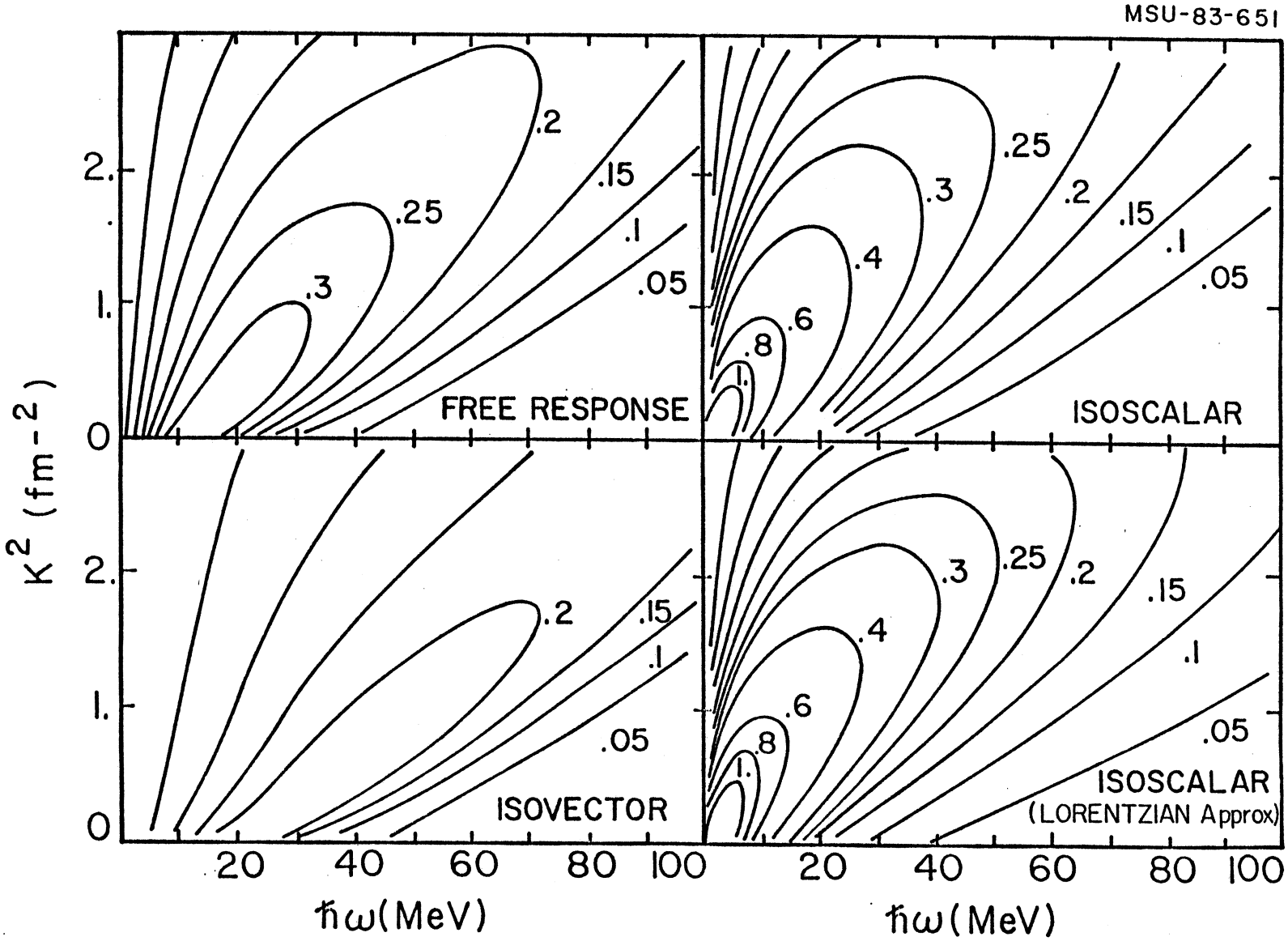
MSU-83-651
FREE RESPONSE
ISOSCALAR
ISOVECTOR
ISOSCALAR
(LORENTZIAN Approx)
K^2 (fm^{-2})
$\hbar\omega$(MeV)
$\hbar\omega$(MeV)
0
1.
2.
20
40
60
80
100
.05
.1
.15
.2
.25
.3
.4
.6
.8
1.

Figure 4

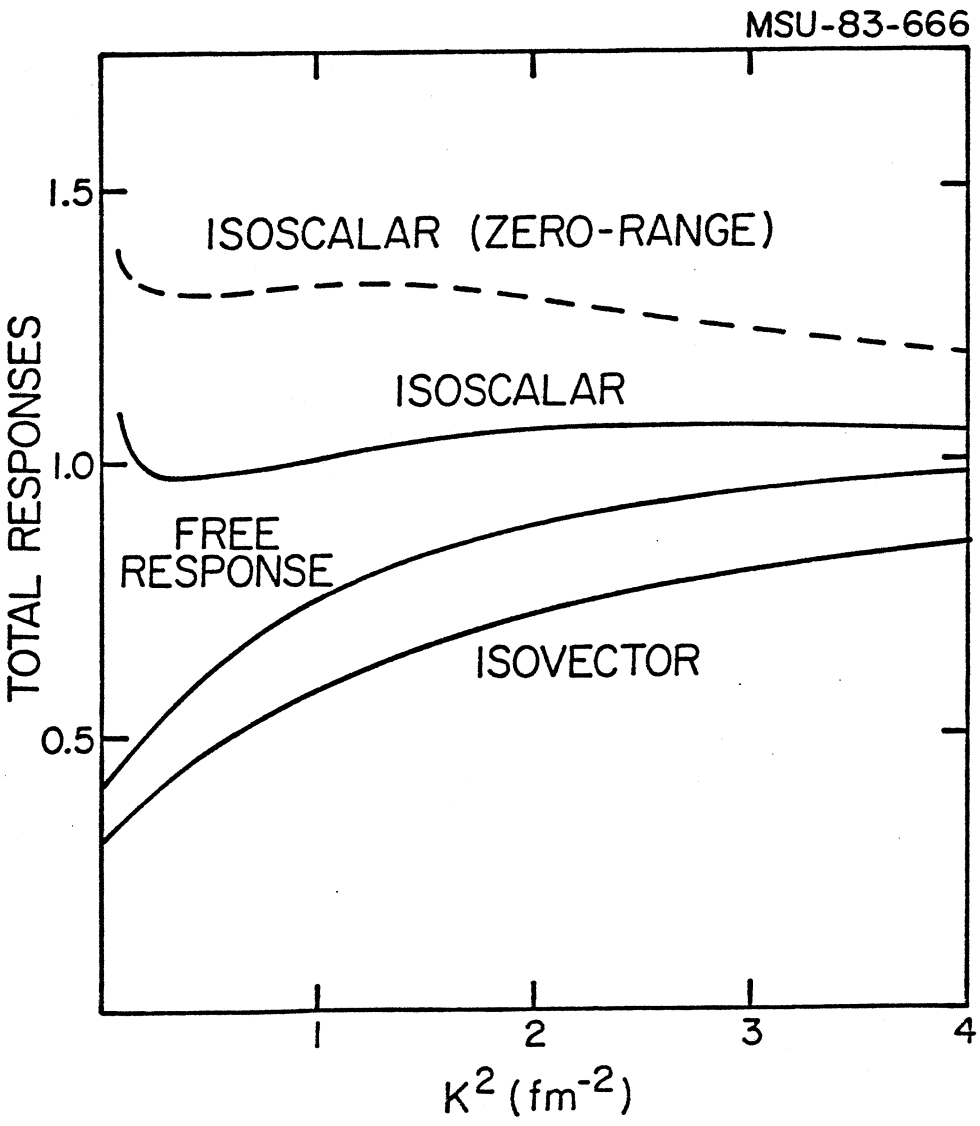
MSU-83-666
1.5
ISOSCALAR (ZERO-RANGE)
ISOSCALAR
1.0
FREE
RESPONSE
ISOVECTOR
0.5
TOTAL RESPONSES
1
2
3
4
K² (fm⁻²)

Figure 5

MSU-83-653

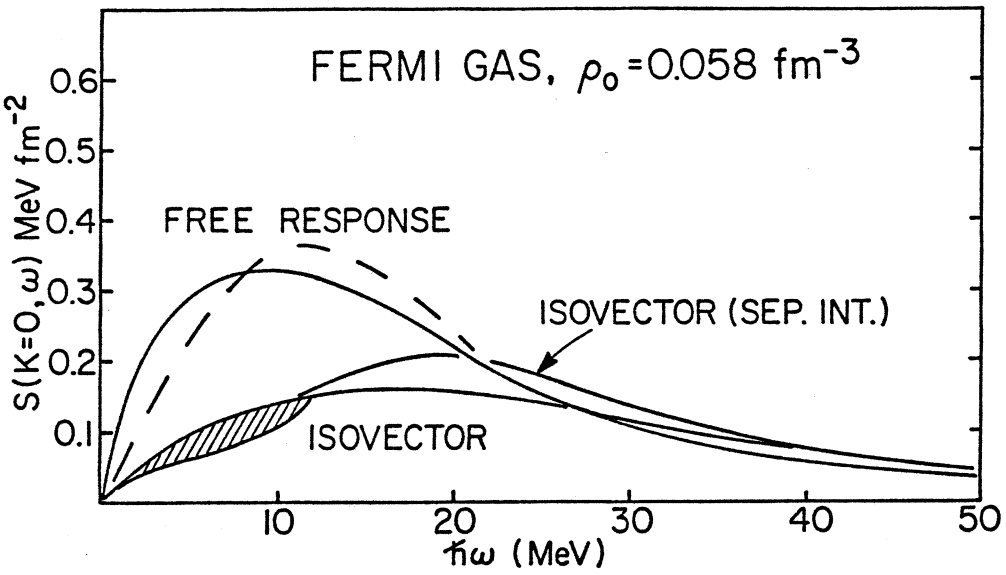

Figure 6

MSU-83-652

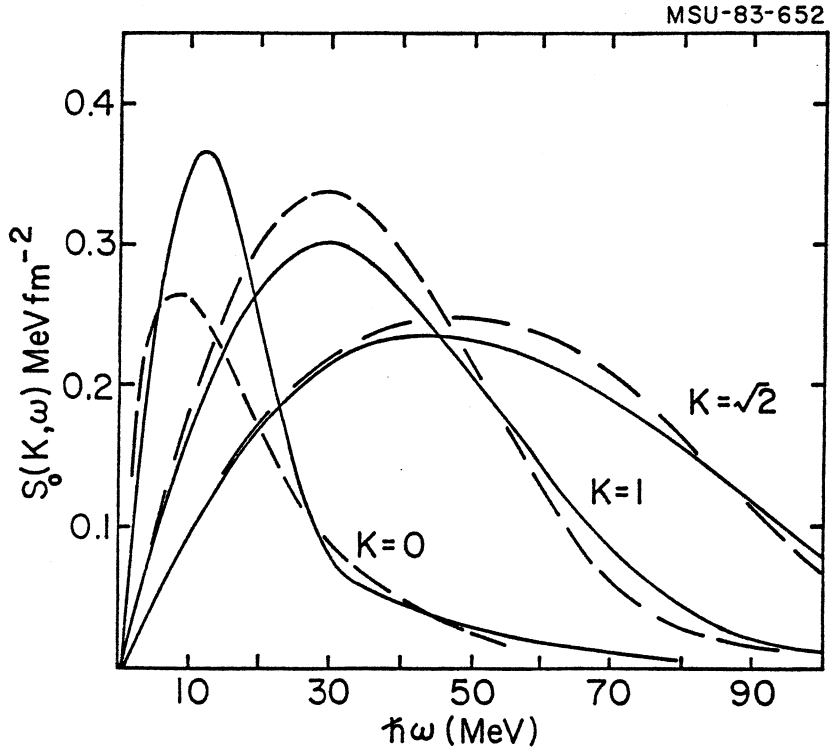

Figure 7

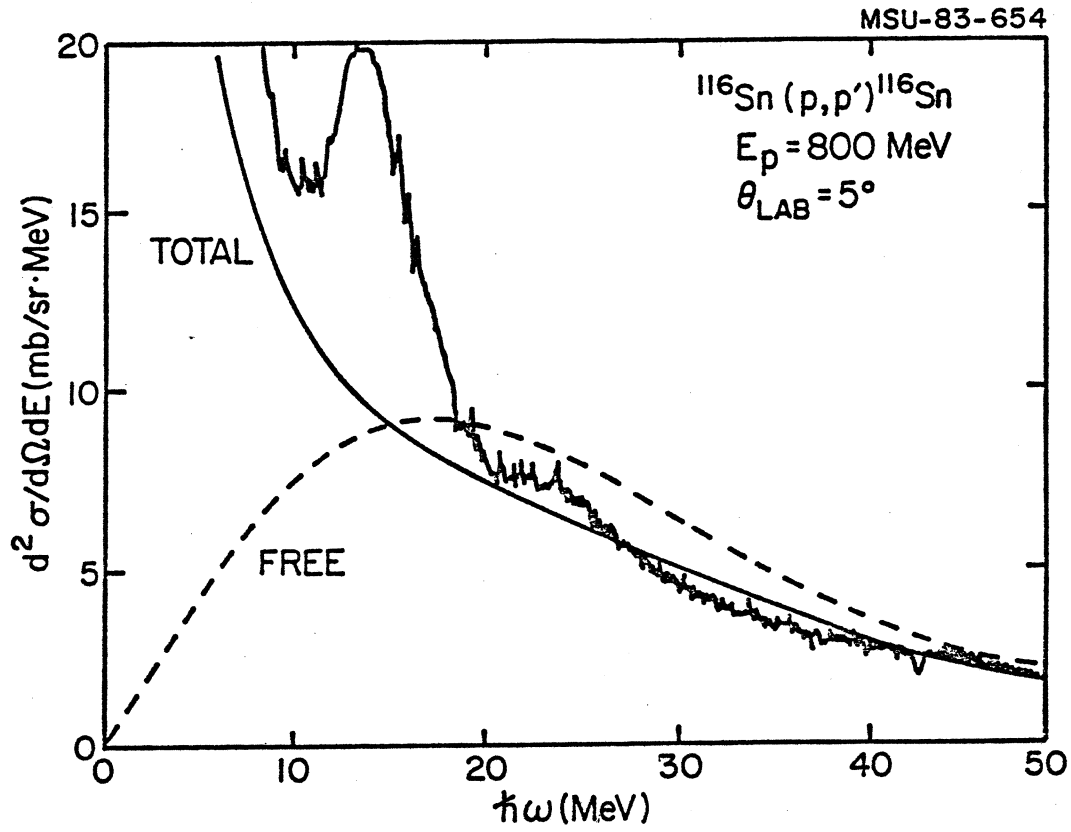

Figure 8

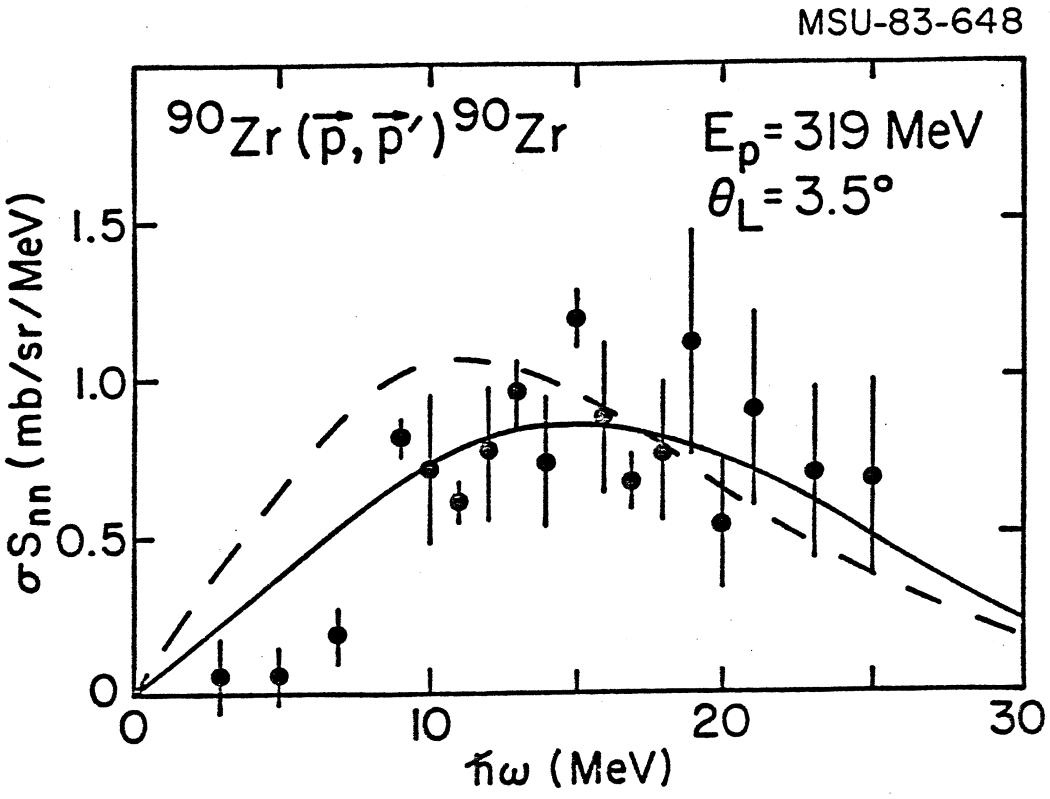

Figure 9